FINITE ELEMENT ANALYSIS OF THE ROLLING RING AND RIDING WHEEL FOR CEMENT ROTARY KILN

Wei WEIHUA[1], Peng YOU[2], Du LIQUAN[3], Li YUANTONG[4], Cai YANING[5], Chen ZENGTAO[6]

The finite element simulation models of the rolling ring and riding wheel were established by using of SolidWorks software. The stress and strain of the rolling ring and riding wheel were analyzed and calculated with finite element method. The simulation results showed that the whole deformation of the rolling ring was it has to be symmetrical; deformation of the top part of the rolling ring was the largest, and the deformation of other parts gradually decreases from the top. The deformation of the riding wheel was not obvious except for the vicinity of the contact area between the rolling ring and riding wheel. In addition, the they have to be symmetrical; again what is new?, the stress and strain values of the outer surface of the rolling ring were smaller than the inner surface at the same angle, and the maximum value of the stress and strain was present on the inner surface of the rolling ring located in the vicinity of contact area between the rolling ring and riding wheel.

Keywords: Cement Rotary Kiln, Rolling Ring, Riding Wheel, Finite Element Analysis.

1. Introduction

The rolling ring and the riding wheel are both important parts of the rotary kiln, which plays the role of supporting the total weight of rotation section of the rotary kiln. Due to supporting huge load, a large contact stress tends to occur in the contact area between the rolling ring and riding wheel. After the operation of the cement rotary kiln for some time, the cracking in the inner and outer surfaces of the rolling ring and the outer surface of the riding wheel, serious wear and other mechanical failure often occur, which will cause process interruption. Therefore, it is of great significance for studying the stress and deformation law of the inner and

[1] College of Mechanical and Electrical Engineering, Nanjing Forestry University, Nanjing, 210037, China, e-mail: whwei@njfu.edu.cn
[2] College of Mechanical and Electrical Engineering, Nanjing Forestry University, Nanjing, 210037, China
[3] College of Mechanical and Electrical Engineering, Nanjing Forestry University, Nanjing, 210037, China
[4] College of Mechanical and Electrical Engineering, Nanjing Forestry University, Nanjing, 210037, China
[5] Jiangsu Hengyuan International Engineering Co. Ltd., Yangzhou, 225266, China
[6] Faculty of Engineering, University of Alberta, Edmonton, T6G 1H9, Canada

outer surfaces of the rolling ring, and the contact stress of the rolling ring and riding wheel as to optimize the structure of the rolling ring and further improve the efficiency of the enterprise.

According to the new type of two stall supporting cement rotary kiln designed by ourselves, the key components of the rotary kiln are simulated and analyzed with ANSYS software. The stress and strain distribution of the rolling ring and riding wheel are obtained, and the weak link of the rotary kiln parts is pointed out, which provides the theoretical basis for the daily inspection and maintenance of the rotary kiln.

2. The structure of rolling ring and riding wheel

The cement rotary kiln consists of the cylinder, rolling ring, riding wheel, transmission system, kiln hood cover, kiln tail cover and other components. The rolling ring, one of the main components of the rotary kiln, is a thick-walled ring. The weight of cylinder and workpiece material of rotary kiln is applied to riding wheel by contact with rolling ring. The riding wheel supports the total weight of rotation section of the rotary kiln, makes the cylinder and rolling ring run smoothly at a low speed. The riding wheel is usually installed at an angle of 30° to the vertical. This research chooses the solid rectangular rolling ring, whose material is the ZG35CrMo. The material of riding wheel is the ZG42CrMo [1, 2]. The material properties are shown in Table 1. The structure of the rolling ring and riding wheel is shown in Fig. 1. A rolling ring is supported by two riding wheels and relies on friction to drive the riding wheel to rotate.

Table 1

The material properties of the rolling ring and riding wheel

Steel Model	Yield Strength σ_s (MPa)	Tensile Strength σ_b (MPa)	Contact Stress P_0 (MPa)	Bending Stress σ_0 (MPa)
ZG35CrMo	(Quenched and tempered) ≥ 510	740～880	400	75
ZG42CrMo	≥ 350	650～800	367	70

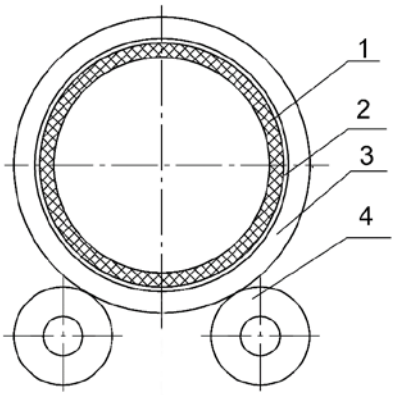

1- firebrick, 2 - steel plate, 3 - rolling ring, 4 - riding wheel
Fig. 1. The structure of rolling ring and riding wheel check figure; it looks like an ellipse and not a circle!

3. The force analysis of the rolling ring

3.1. Assumptions before analysis

Due to the complex working conditions of the rotary kiln, in order to simplify the analysis process and ensure the calculation accuracy of contact stress between the rolling ring and riding wheel, the following assumptions are made [3, 4].

(1) Although the temperature inside the rotary kiln is very high, the external temperature is relatively low, and the temperature difference between the inner and outer surface temperature of the rolling ring is very small, so the thermal stress can be neglected when analyzing the rolling ring and riding wheel model.

(2) The weights of kiln baffle, kiln head and kiln tail seal are very small compared total weight of the assembly (no more than 1%), so the calculation only considers the weight of the rotary kiln key components.

(3) The rotation speeds of the rolling ring and riding wheel are very low (about 0.2 rot/min), so the centrifugal forces can be ignored.

3.2. The force analysis of the rolling ring

The rolling ring is looped in the cylinder. There are generally 24 to 42 plates per cylinder of the rotary kiln. The total length of contact part between the rolling ring and cylinder accounts for about 70% give notation from figure! of the entire circumference, so the contact between the rolling ring and cylinder can be regarded as a continuous contact. The load distribution of the rolling ring is shown in Fig. 2.

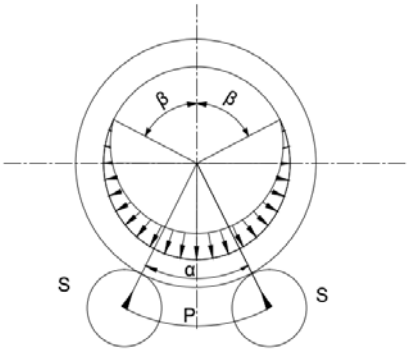

Fig. 2. The load distribution of the rolling ring section

As it can be seen from the above figure, the pressure load applied to the rolling ring is of cosine distribution. The pressure distribution on the rolling ring can be obtained as follows [5]:

$$P = \frac{Q}{\pi R_c}(\lambda - \cos\alpha) \tag{1}$$

Equation: P - the pressure distribution of the rolling supporting surface, Pa

Q - the maximum support force, N,

α - pressure distribution angle, °,

R_C - the centroid circle radius of the rolling ring, m,

λ - coefficient related to the angle β; its relationship is [3]:

$$\lambda = \frac{1}{2}\left(\frac{\beta}{\sin\beta} + \cos\beta\right) \tag{2}$$

where β - the contact angle [°].

In the design of the reaction rotary kiln, taking β=27°, Q=7066300N, Rc=2.936 m, then putting into the equation (2): λ=0.88.

The final result is

$$P = 7066300 \times \frac{(0.88 - cos\,\theta)}{2.936^2\pi} Pa \tag{3}$$

4. Finite element analysis of the rolling ring and riding wheel

4.1. The model of the rolling ring and riding wheel

The model established for the rolling ring and riding wheel, and the global coordinate system (GCS) are shown in Fig. 3. The X is the axial direction and the Z axis is vertically upward. The main parameters of the rolling ring and riding wheel are shown in Table 2, [6].

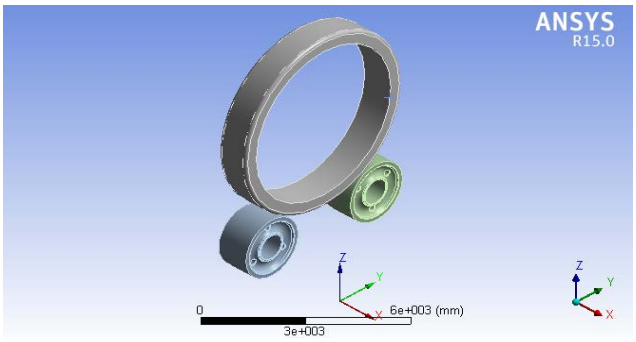

Fig. 3. The model of the rolling ring and riding wheel

Table 2

The main parameters of the rolling ring and riding wheel

Serial number	Name	Material	Width (mm)	Thickness (mm)	Aperture (mm)	Elastic modulus (Pa)	Poisson's ratio	Density (kg/m^3)
1	Rolling ring	ZG35CrMo	1150	438	N/A	2.09E11	0.291	7860
2	Riding wheel	ZG42CrMo	1200	N/A	830	2.09E11	0.3	7860

4.2. Defining the contact surface

As for other static analyses, the contact analysis also requires setting the properties of the material, except that the contact is defined before the mesh is divided. If the number of contact pairs is greater than or equal to 2, the pair must be named or numbered. The interaction between the rolling ring and riding wheel is a contact problem between two flexible bodies.. Generally, the surface with smaller area is defined as contact surface, and the surface with larger area is defined as target surface. The result is shown in Fig. 4.

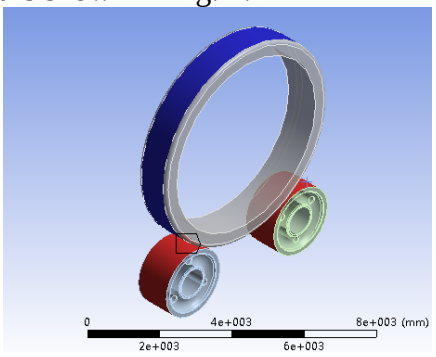

Fig. 4. The definition of contact surface

Therefore, the surface on the riding wheel is defined as the contact surface, and the surface on the rolling ring is defined as the target surface [7, 8].

4.3. The choice of contact algorithm

When the surfaces of two different objects are in contact and tangent, then the two objects can be called contact. When the two objects form the contact, the contact surface of the two objects can be free to separate along the normal or move along the tangential direction each other, and can't permeate each other. The contact surface of two objects can transfer normal compression pressure and tangential friction each other, but can't pass the normal tensile force. The contact between two physical surfaces must have a specific relationship to complete the contact analysis, and ANSYS Workbench provides several contact algorithms [9-11]: Pure Penalty, Normal Lagrange, Multi-point Constraints, Augmented Lagrange.

For the surface contact of two different objects, the Pure Penalty method will first see whether there is penetration between the contact surfaces before the calculation, not clear, please rephrase! needs to introduce a normal contact stress $\boldsymbol{F_N}$ between contact surfaces ($\boldsymbol{F_N = K_N x}$, $\boldsymbol{K_N}$ is the normal contact stiffness, x is the tangential depth). The accuracy of the calculation is related to the magnitude of the contact stiffness. The higher the $\boldsymbol{K_N}$, the higher the accuracy. Being different from the Pure Penalty method, the Normal Lagrange method takes contact force as an not clear, please rephrase! , which is an accurate contact algorithm. However, due to the increase of the degrees of freedom, the computational efficiency will be lowered, and the vibrations will appear if the contact state abruptly changes. The Augmented Lagrange method adds an additional contact force $\boldsymbol{\lambda}$ ($\boldsymbol{F_N = K_N x + \lambda}$) as compared to the Pure Penalty method, so the change in the contact stiffness is not as sensitive as for Pure Penalty method. Compared to the Augmented Lagrange model, the Normal Lagrange model needs to add the contact trajectory to the model, which will increase the computational cost. The Multi-point Constraints are a way of directly contacting the related interface of the bound area by adding a constraint equation to connect the displacement of contact surfaces, then to obtain the normal contact stress, which is similar to the one obtained from the Pure Penalty. Considering the efficiency of the Augmented Lagrange method, and the accuracy of the contact stress analysis of the rolling ring and riding wheel model, the Augmented Lagrange method is selected in this paper.

4.4. Establishing the mesh

The local refinement option is used to encrypt the mesh at the points of contact when the plane model is meshed [12-16]. The mixed tetrahedron and hexahedral meshing methods are used in the contact area while the not clear, please rephrase! is used in other areas. The result of the meshing is shown in Fig. 5, the total number of elements is 28217, and the total number of nodes is 50002.

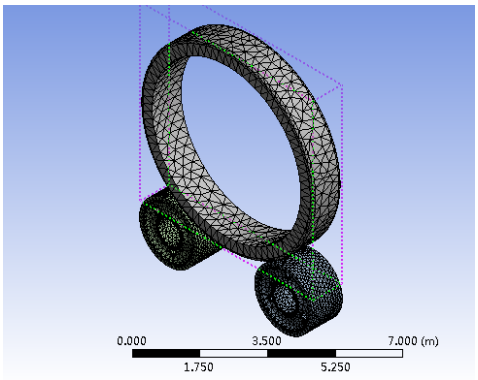

Fig. 5. The mesh of the whole model

4.5. Constraints and loads

. The constraints in ANSYS are treated as a load, that is, they can be applied to objects such as points, lines, faces, bodies, and the nodes and elements of the finite element analysis (FEA) model. The constraints applied to the analyzed model of the rolling ring and riding wheel are shown below:

(1) The points of inner surface of the rolling ring in the GCS coordinate system are 0 in the translation and rotation about the X direction, 0 in the translation along Y direction, and 0 in the rotation about the Z direction.

(2) The points of the inner surface of the two riding wheel holes in the GCS coordinate system are 0 in the translation and rotation about the X direction, 0 in the translation along Y direction, and 0 in the translation and rotation about the Z direction.

A total of two loads are applied, one is the pressure load on the inner surface of the rolling ring, and the other is the gravitational load. A suitable cylindrical coordinate system is created when the rolling ring pressure load is applied. The applied loads and constraints are shown in Fig. 6 and Fig. 7, respectively.

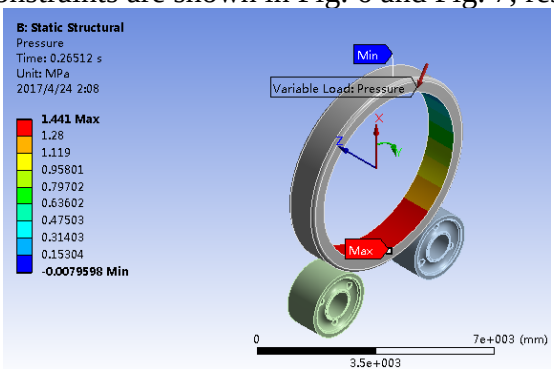

Fig. 6. Model of loads

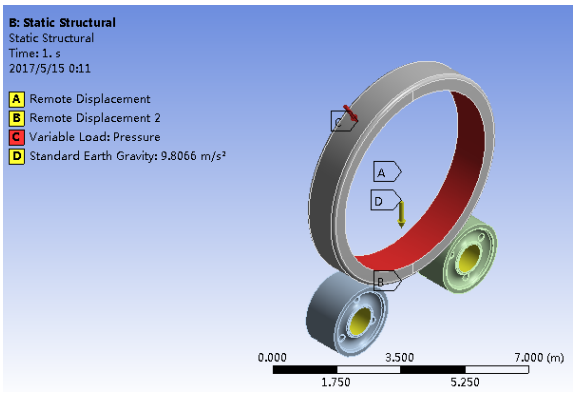

Fig. 7. Model of constraints

5. Results and analysis

5.1. Deformations analysis

The results can be viewed with the overall deformation shown in Fig. 8. From this figure, we can clearly see that the overall deformation of the rolling ring is larger than that of the ring wheel. The top deformation of the rolling ring in the structure field is the largest, the maximum value is 2.821 mm, and the deformation of other parts gradually decreases from the top.

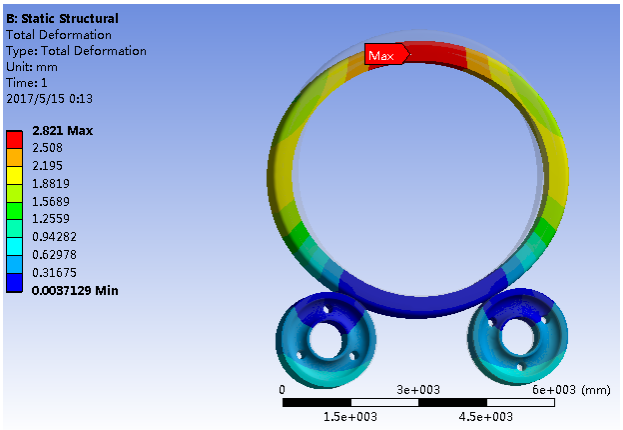

Fig. 8. The total deformation of the rolling ring and riding wheel contact model

5.2. Model stresses and strains

The results are shown in Fig. 9 and Fig. 10, respectively. It can be seen from the figures that the maximum equivalent stress value and strain value both appear on the inner surface of the rolling ring where locates the vicinity of the contact area between the rolling ring and riding wheel, are symmetrical about the plane XOZ.

The maximum this is a displacement and not a strain! Give a strain value as 542 μm/m! Why don't you start with stresses from Fig. 9 and afterwards talk about strain from Fig. 10?, and the maximum stress value is 65.122 MPa which is within the allowable bending stress σ range of the riding wheel (σ_0=75 MPa, the safety factor is 1.1 [5]).

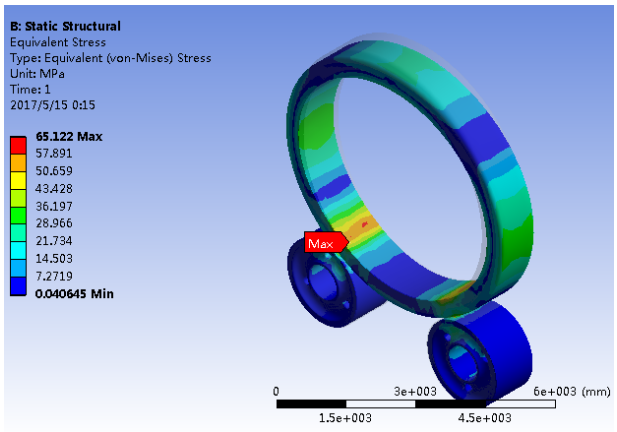

Fig. 9. The equivalent stress cloud chart of the rolling ring and riding wheel contact model

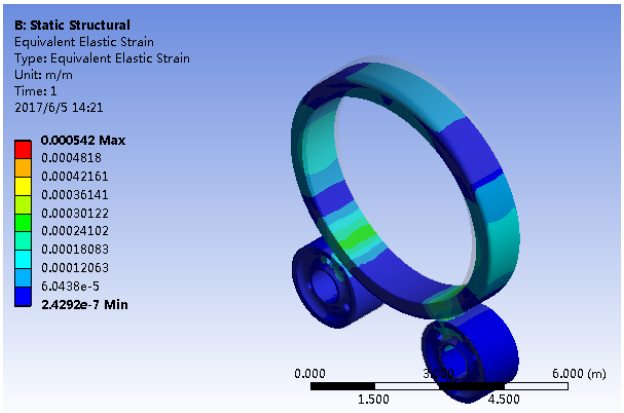

Fig. 10. The equivalent strain cloud chart of the rolling ring and riding wheel contact model

The path analysis method in the post-processing of ANSYS Workbench is an effective way to show the stresses and strains resulting in the model. There are often two steps. The first step is to create the path, and the second step is to map the stresses and strains of the model to the corresponding path. The stresses and strains of the rolling ring are symmetrical about the XOZ plane, so the path created is only half a circle. Two paths were created, as shown in Fig. 11. The paths located in the middle of the inner and outer surfaces of the rolling ring where the starting point is at the top of the rolling ring ("1" in Fig. 11, the angle is 0°) and the end is at the bottom of the rolling ring ("2" in Fig. 11, the angle is 180°).

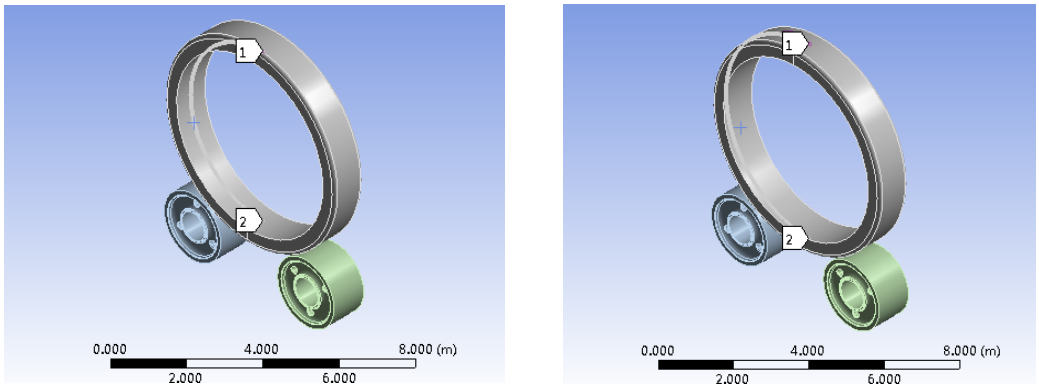

(a) inner surface

(b) outer surface show better the outer surface on the right of the rolling ring as to be seen better!

Fig. 11. The surface path chart of the rolling ring

Fig. 12 and Fig. 13 are plotted the equivalent stress and equivalent strain curves in the circumferential direction of the inner surface of the rolling ring, respectively. It can be seen from Fig. 12 and Fig. 13 that the maximum of equivalent stress and equivalent strain both appear on the inner surface around 150° of the rolling ring where is the vicinity of the contact area between the rolling ring and riding wheel. The maximum value of the equivalent stress is 52.74 MPa, and the maximum value of equivalent strain is 0.253 mm.

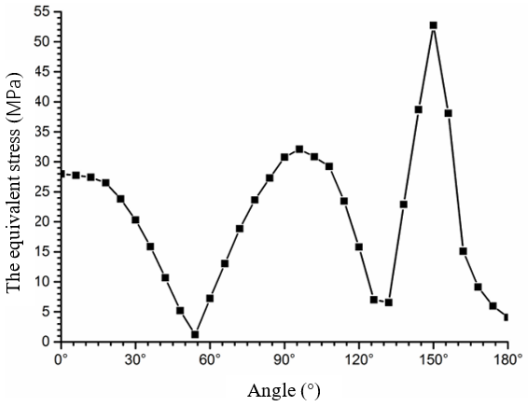

Fig. 12. The equivalent stress curve chart on the inner surface of the rolling ring

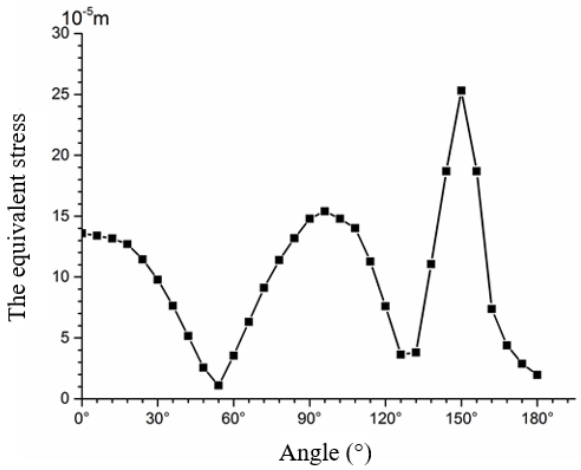

Fig. 13. The equivalent strain the legend of the vertical axis is “stress” curve chart on the inner surface of the rolling ring

Fig. 14 and Fig. 15 present the equivalent stress and equivalent strain curves of the outer surface of the rolling ring, respectively. It can be seen from Fig. 14 and Fig. 15 that the maximum of equivalent stress and equivalent strain both appear on the outer surface nearing 150° of the rolling ring where is the vicinity of the contact area between the rolling ring and riding wheel. The maximum stress is 34.59 MPa, the maximum strain is 0.195 mm. By comparing the stress and strain values of the inner and outer surfaces of the rolling ring, it can be found that the strain and stress value of the inner surface of the rolling ring are larger than those of the outer surface of the rolling ring when the angle is same.

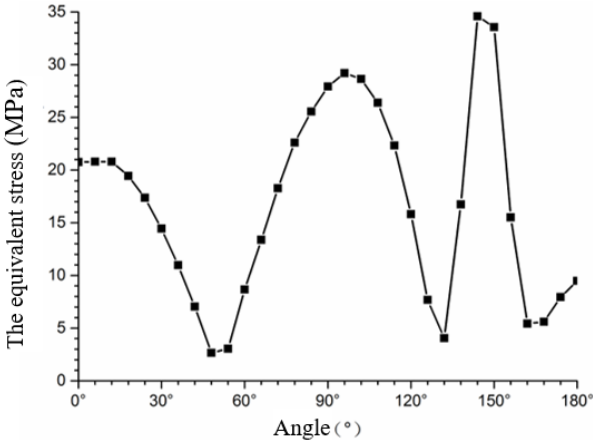

Fig. 14. The equivalent stress curve chart on the outer surface of the rolling ring

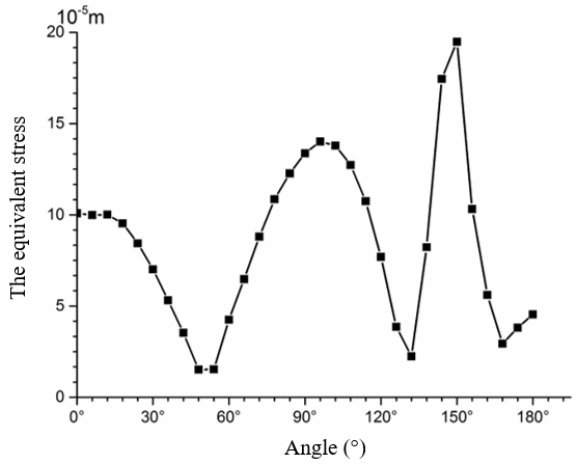

Fig. 15. The equivalent strain the legend of the vertical axis is “stress” curve chart on the outer surface of the rolling ring

Explain what happens around 56 º and 128 º!!!

5.3. Stress distribution of contact surfaces

Adding “Contact Tool” command in “Solution” and solving, the result is shown in Fig. 16.

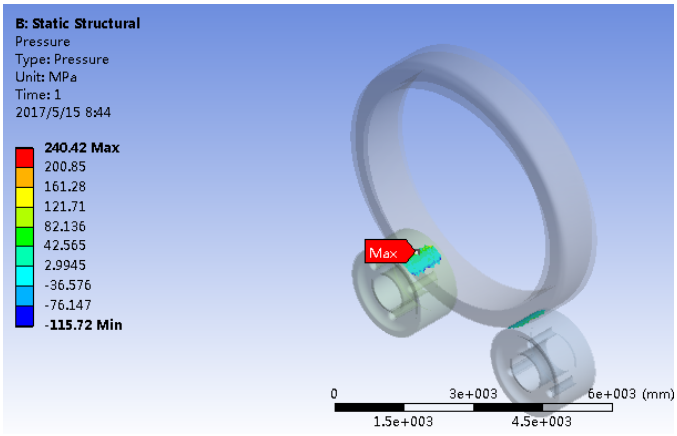

Fig. 16. The stress chart in the contact surface between the rolling ring and riding wheel

The stress distribution of the model intuitively reflects the stress change at each position of the contact process. The stress reaches the peak in the contact center of the left rolling ring and the maximum contact stress is 240.42 MPa which is within the allowable contact stress $\boldsymbol{p_0}$ range of the riding wheel ($\boldsymbol{p_0}$=367 MPa), which proves that the design of the rolling ring and riding wheel is reasonable. The

rolling ring relies on friction to drive the rotation of the riding wheel, and with the increase of working hours, the wear in the contact area between the rolling ring and riding wheel will increase, some phenomena such as the pitting or peeling may happen on the surface of the riding wheel, which will seriously affect the service life of the riding wheel and cause the wheel can't run properly. Therefore, in order to ensure the normal operation of the kiln, the surface quality of the rolling ring and riding wheel should be often checked after the rotary kiln is running for some time.

6. Conclusions

The finite element simulation model of the rolling ring and riding wheel contact is established by using of SolidWorks software. The contact algorithm is defined with the Augmented Lagrange method. The local refinement method is adopted to divide the mesh. The contact stress of the rolling ring and riding wheel is analyzed and calculated by using of finite element method. this is known and not advanced! Pathway analysis is used to analyze the stresses and strains resulting in the rolling ring, and the which is this curve? The dangerous area of the rolling ring is pointed out, which provides the basis for the daily inspection of the rolling ring. The following conclusions can be drawn:

(1) The top deformation of the rolling ring is the largest, and the deformation of other parts gradually decreases from the top. The overall deformation of the rolling ring is larger than that of the ring wheel, and the deformation of the riding wheel not clear, please rephrase! except for the vicinity of the contact area between the rolling ring and riding wheel.

(2) The stress and strain on the outer surface of the rolling ring are less than those of the inner surface of the rolling ring when the angle is same. The maximum of equivalent stress and equivalent strain of the rolling ring both appear on the position of inner surface of the riding wheel where locates the vicinity of the contact area between the rolling ring and riding wheel.

(3) The contact stress analysis showed that the maximum value of the contact stress between the rolling ring and the riding wheel appears at the center of the contact area. It is necessarily to regularly and effectively detect the contact area, and the detected results can provide a basis for changing the rolling ring and riding wheel.

Acknowledgement

The authors are grateful for the financial support from the Open Fund for Jiangsu Province Key Laboratory of Advanced Manufacturing Technology (HGAMTL-1605), the Joint Training Demonstration Base Construction Project for Professional Degree Graduate in Nanjing Forestry University (2017JD01), Jiangsu "Six Talent Peak" Project (JXQC-

022), and Jiangsu Overseas Research Training Program for Prominent Young & Middle-aged Teachers and Presidents in Colleges and University.

REFERENCES

[1]. *X. Tang, B. Wang, H. Zhang, X.B. Fu, H.C. Ji*, "Study on the microstructure evolution during radial-axial ring rolling of IN718 using a unified internal state variable material model", in International Journal of Mechanical Sciences, **Vol. 128-129**, 2017, pp. 235-252.

[2]. *L. Hua, J.D. Deng, D.S. Qian, J. Lan, H. Long*, "Modeling and application of ring stiffness condition for radial-axial ring rolling", in International Journal of Machine Tools & Manufacture, **vol. 110**, 2016, pp. 66-79.

[3]. *R. Saidur, M.S. Hossain, M.R. Islam, H. Fayaz, H.A. Mohammed*, "A review on kiln system modeling", in Renewable and Sustainable Energy Reviews, **Vol. 15**, 2011, pp. 2487-2500.

[4]. *K. Pazand, M.S. Panahi, M. Pourabdoli*, "Simulating the mechanical behavior of a rotary cement kiln using artificial neural networks", in Materials and Design, **Vol 30**, 2009, pp. 3468-3473.

[5]. *F.S. Wang*. Basic Knowledge of Modern Cement Production [M]. China Building Materials Industry Press, 2004: 40-126

[6]. *G.R. Hua, Y.C. Wang, W.H. Li*, "Contact analysis of Type17 coupler based on finite element method", in Engineering Failure Analysis, **vol. 77**, 2017, pp. 23-30.

[7]. *W.H. Wei, J.H. Xu, Y.C. Fu, S.B. Yang*, "Tool Wear in Turning of Titanium Alloy after Thermohydrogen Treatment", in Chinese Journal of Mechanical Engineering, **vol. 25**, 2012, pp. 776-780.

[8]. *F. Hokes, J. Kala, M. Husek, P. Kral*, "Parameter Identification for a Multivariable Nonlinear Constitutive Model inside ANSYS Workbench", in World Multidisciplinary Civil Engineering-Architecture-Urban Planning Symposium 2016, ???? 2016, **vol. 161**, 2016, pp. 892-897.

[9]. *D.R. Van Puyvelde*, "Simulating the mixing and segregation of solids in the transverse section of a rotating kiln", in Powder technology, **Vol. 164**, 2006, pp. 1-12.

[10]. *Q. Yin, W.J. Du, X.L. Ji, L. Cheng*, "Optimization design and economic analyses of heat recovery exchangers on rotary kilns", in Applied Energy, **Vol. 180**, 2016, pp. 743-756.

[11]. *J.C. Díaz, F.R. Mazón, P.G. Nieto, F.S.D. Domínguez*, "Design and finite element analysis of a wet cycle cement rotary kiln", in Finite Elements in Analysis and Design, **Vol. 39**, 2002, pp. 17-42.

[12]. *W.H. Wei, Y.T. Li, T.M. Xue, S.Y. Tao, C.T. Mei, W.D. Zhou, J. Wang, T.Y. Wang*, "The Research Progress of Machining Mechanisms in Milling Wood-based Materials", in Bioresources, **vol. 13**, 2018, pp. 2139-2149.

[13]. *A. Parvizi, K. Abrinia*, "A two dimensional upper bound analysis of the ring rolling process with experimental and FEM verifications", in International Journal of Mechanical Sciences, **vol. 79**, 2014, pp. 176-181.

[14]. *J. Liu*, Explanation of Mechanical Simulation Examples in ANSYS 14.5 Workbench [M]. Machinery Industry Press, 2015: 30-120.

[15]. *C.X. Huang, C.Z. Liu*, ANSYSWorkbench14.0 Super Learning Manual, People Post Press, China, 2013.

[16]. *N.A. Stoica, A. Tudor*, "Experimental results about the stick-slip phenomenon with application to the disc-brake friction materials couple used in the automotive domain", in UPB Scientific Bulletin, Series D: Mechanical Engineering, **Vol. 80**, 2018, pp. 155-170.